NASA Technical Memorandum 106195

Laser Velocimeter Measurements of the Flow Field Generated by a Forward-Swept Propfan During Flutter

Gary G. Podboy and Martin J. Krupar
Lewis Research Center
Cleveland, Ohio

Prepared for the
24th AIAA Fluid Dynamics Conference
Orlando, Florida, July 6–9, 1993

NASA

Laser Velocimeter Measurements of the Flow Field Generated by a Forward-Swept Propfan During Flutter

Gary G. Podboy and Martin J. Krupar
National Aeronautics and Space Administration
Lewis Research Center
Cleveland, Ohio 44135

SUMMARY

Results are presented from an investigation to measure the flow field generated by a forward-swept propfan operating in flutter at a low forward velocity. For comparison to the flutter condition, flow field data are also presented for a slightly reduced rotational speed just below flutter. The forward-swept propfan was tested as the front rotor of a counterrotating pusher propeller. A laser Doppler velocimeter (LDV) was used to measure the velocity field in planes normal to the model centerline downstream of the rotor and in planes of constant radius within the blade passages at each operating condition. A comparison of the data taken at the two different operating conditions indicated that the mean, time-averaged flow about the blades did not change drastically as the propfan rotational speed was increased from the stable operating point to the flutter condition. No regions of flow separation could be identified in the data plots of the mean intrablade flow field. The data also indicate that the relative flow about the blades remained subsonic during flutter operation. The blades were found to have a higher than expected tip loading at both operating conditions. This is thought to have been caused by the outer blade sections twisting under load to higher than expected effective blade angles. This high tip loading resulted in strong vortices and a very nonuniform flow downstream of the tips of the forward-swept blades. This high tip loading may also have caused the blade flutter.

INTRODUCTION

Since the mid 1970's, propfans have been investigated as a means of powering aircraft at high subsonic speeds. Advanced propeller models have been tested in wind tunnels to quantify the effects of varying such propeller design parameters as blade shape, number of blades, and inflow Mach number on the overall aerodynamic and acoustic properties of both single rotating and counterrotating configurations. The rotor blades used in these models are normally swept aft (opposite the flight direction), to take advantage of acoustic and aerodynamic benefits which result from the use of blade sweep at cruise operating conditions. To provide an acoustic benefit, the sweep is tailored to reduce noise through phase cancellation of thickness and loading noise harmonics. The aerodynamic benefit arises from decreased shock losses at the blade tips which operate transonically at cruise. Propfans have been shown to have a significant aerodynamic performance advantage relative to current turbofans at typical cruise conditions of Mach 0.8 and 35,000 feet altitude.

The counterrotating propellers that have been tested are inherently more fuel efficient than the single rotation propellers due to the ability of the downstream rotor to redirect the swirl generated by the front rotor back into the axial direction. Unfortunately, the counterrotating configurations are also inherently noisier than the single rotation propellers. Much of the increased noise for the counterrotating case occurs because the downstream rotor operates in the highly unsteady wake flow set up by the front

sweep would allow the formation of a leading edge vortex which could prevent the separation.

Recently a test was conducted in the NASA Lewis 9' X 15' Wind Tunnel of a forward–swept rotor which had 30 degrees of leading edge sweep over the outer 40% of the blade span. The initial purpose of this test was to determine if, at simulated takeoff conditions, these forward–swept blades would provide a more uniform wake flow than the aft–swept blades normally used in these counterrotating propfans. As part of this investigation, laser Doppler velocimetry (LDV) was used to measure the rotor wake characteristics of both this forward–swept rotor and a reference aft–swept rotor. The velocity field created by the aft–swept rotor was measured in several axial planes downstream of the rotor while operating at low and moderate power levels. A similar set of wake data was obtained downstream of the forward–swept blades only at low power since they fluttered at higher power conditions.

Due to the flutter, the emphasis of the laser velocimetry testing shifted from determining the rotor wake flow characteristics to measuring the flow field around the forward–swept blades during flutter. It was anticipated that the detailed flow field data obtainable with the laser velocimeter might identify an aerodynamic excitation mechanism which caused the flutter. One possibility was that the flutter was initiated by flow separation from the blades. This could be a blade pressure or suction surface separation, or in the form of a tip or leading edge vortex. Another possibility was that shock waves resulting from supersonic relative flow on the blades were causing the flutter. In an effort to identify an excitation mechanism, the LDV surveys conducted in support of the flutter investigation concentrated on measuring the near field flow within and just downstream of the blade passages. It was thought that the intrablade data would be especially valuable in determining the cause of the flutter. This data could be used to identify if flow separation had occurred and/or the likelihood of having any regions of supersonic relative flow in the vicinity of the blades.

This data was also obtained for the purpose of generating a data base that could be used to verify the output of computational codes which have been developed to predict flutter. For reliable flutter predictions, it is necessary to accurately represent both the flow about the blades and the structural characteristics of the blading. Unfortunately, if there is some discrepancy between code predictions and experiment, there is normally little information available to determine if the fault lies with the theoretical models of the flow field or the models of the blade structure. The detailed velocity data obtained during this test can be used to quantify the ability of a code to simulate the mean, time–averaged flow about the blades during flutter.

The purpose of this paper is to present LDV measured velocity data obtained during this flutter testing. This is believed to be the first laser velocimeter data obtained on the flow field produced by an unducted rotor during flutter. Data is presented for two model operating conditions at a freestream velocity of Mach 0.2 – an rpm condition at flutter, and a condition at which the rpm was reduced just enough to get out of flutter. Data was obtained at the same locations relative to the model at each of the conditions, thus permitting the two flow fields to be compared. Data is presented which depicts the flow field occurring just downstream of the forward–swept front rotor blades at each of the two operating conditions. Data depicting the flow within the blade passages at the two conditions is also presented and compared. A discussion of the apparent cause of the flutter and of the significance of various wake flow non–uniformities in the production of interaction noise is also provided.

corresponding front rotor advance ratios (J) were 1.07 and 1.127 at 5900 and 5600 RPM, respectively.

Laser Velocimeter System and Data Acquisition

The laser Doppler velocimeter (LDV) used was a four–beam, two–color, backscatter system which permitted the measurement of two components of velocity simultaneously. Two green beams were used to measure the axial components of velocity, while two blue beams allowed the measurement of radial and tangential components. Axial and radial velocities were measured above the model in a vertical plane passing through the model centerline. Axial and tangential components were measured in a horizontal plane on the side of the model (fig 3). The LDV probe volume, which was ellipsoidal in shape, had a diameter of approximately 0.11 mm (0.0043 in) and was roughly 6.0 mm (0.24 in.) long.

The tunnel flow was seeded with polystyrene latex (PSL) spheres manufactured at the NASA Lewis Research Center to be less than or equal to one micron in diameter. Due to the manufacturing process, these solid particles are supplied suspended in water. Before introduction into the tunnel this solution is diluted by mixing it with 200 proof ethyl alcohol. This solution was then sprayed into the tunnel at a location 80 feet upstream of the test section. The liquid evaporates in the time it takes to reach the model, leaving behind the solid PSL seed on which the LDV data was obtained.

Figure 4 illustrates the axial and radial locations relative to the model at which data were obtained during LDV runs conducted to support the flutter investigation. Figure 4a shows measurement locations for the flutter operating condition, while figure 4b gives locations for the below flutter condition. Data were acquired by making either radial traverses of the measurement volume at a constant axial location or axial traverses at a constant radial location. All three velocity components were measured in the constant axial planes labeled in the figure as stations 1A and 2A. Station 1A and 2A are 0.53 and 1.79 inches, respectively, downstream of the pitch change axis of the front rotor blades. For most of the measurement locations within these two planes, the axial velocities were measured twice – once in the vertical plane above the model and once in the horizontal plane on the side. For the constant radial intrablade surveys only axial and tangential components were measured. In order to measure radial velocities with this LDV system, it was necessary to position the measurement volume in the vertical measurement plane above the model. When positioned to obtain data inside the blade passages in this plane, the blades blocked access to the required measurement locations, making it impossible to measure the radial velocities.

Shaft angle encoders, coupled with once–per–revolution signals from the rotors, were used to determine the angular position of each rotor whenever a velocity measurement was made. Two encoders were used for each of the two velocity components being measured. One of these two encoders was fed with the once–per–rev signal from the front rotor, while the other encoder received the signal from the aft rotor. These encoders segmented the 360 degrees of rotor revolution occurring between two consecutive once–per–revolution pulses into 720 bins. Each time a velocity measurement was made, each of the two encoders corresponding to that velocity component was sampled to determine the number of bins generated since the occurrence of the previous once–per–rev pulse. These bin numbers reference the velocity measurement relative to the circumferential location of the blades of each rotor.

Data were acquired at each location over many rotor revolutions until a sufficient amount of data had been obtained to accurately resolve the flows occurring within the individual blade passages. The data were acquired in "random" mode, meaning that the two LDV channels obtained data independently.

to provide a better view of any transitions which may occur across the boundaries of the passage. One quadrant of a complete rotor flow field is illustrated. The axial velocities are represented in the figure by the color contours; the plotted vectors depict the secondary velocities determined by vectorially adding the phase–locked averaged radial and tangential velocities measured at equivalent locations relative to the propeller blades. Secondary velocities are not plotted for radial locations less than 11.25 inches since radial components could not be measured within the blade passages.

Several flow field features can be identified in figure 6. Vortices trailing from the tips of these blades are evident from the clockwise swirl of the secondary velocity vectors downstream of the blade tips and by the rapid change in axial velocity which occurs as one proceeds radially through these regions. The velocity perturbations occurring due to these vortices are significantly higher than those which occur anywhere else in the flow field. Phase–locked averaged axial velocities ranging from 40 to 560 ft/sec and phase–locked averaged radial velocities ranging from +110 to −270 ft/sec were measured within these vortices. These data indicate that a very nonuniform wake flow was generated by the tips of these forward–swept blades. The viscous blade wakes shed from the outer portions of the blades show up in the color contours as dark green radial lines spanning in radius from r=11.0 to r=12.0 inches. The secondary velocity vectors (computed from the vector sums of the radial and tangential components) reveal increased tangential velocities within the blade wakes, indicating a strong tendency for this viscous flow to be dragged along in the direction of rotation of the blades. The narrow width of the wake suggests that upstream of the blade trailing edge the flow was attached to the blade surface. The axial velocity contours plotted for the intrablade radial locations (r<11.0 in) also depict a normal, attached mean flow. These contours do not rule out the possibility that the flow did separate from the blades; it is possible that the flow separated upstream of this axial location and then re–attached. They do suggest, however, that if separation occurred, it was not massive, and that the flutter was not caused by massive blade stall.

Figure 7 shows the phase–locked averaged velocities measured during flutter (5900 rpm) at axial station 2A (just downstream of the front rotor trailing edge). In this plane axial velocities were measured further inboard than at station 1A, with the innermost radial location within 0.2 inches of the hub surface. A complete set of secondary velocities could not be measured at the innermost radial locations since at some angular orientations of the front rotor the blades blocked the view of the optics used in the measurement of these components. The axial velocity contours show the boundary layer which forms along the centerbody and the deficits occurring within the viscous blade wakes over the entire blade span. The viscous blade wakes are shown to be relatively wide over the outer portions of the blade span, between the radial locations of 8.5 and 11.5 inches. Wider wakes are expected at these outer radial locations due to the spreading which occurs as the wakes convect downstream. Because of the forward sweep of the front rotor blades, the outer measurement locations are further downstream of the blade trailing edges. Consequently, the wakes measured further outboard have had more time to spread circumferentially. It is worth noting the lack of any significant perturbation in the axial velocity contours due to a hub vortex. This indicates that if a hub vortex did form it is much weaker than the tip vortex and, therefore can be expected to contribute much less to the generation of interaction noise.

It was suspected that the manner in which the data was reduced might also be responsible for some of the increase in the wake width shown at the outer radial locations. Due to the time–averaging effect of the data reduction process, thin, oscillating wakes would be smeared circumferentially and appear wider in these plots. However, similar increases in the wake width were found for each of the other operating conditions at which LDV data were obtained downstream of the forward–swept rotor. This includes two nonflutter conditions other than the below flutter condition discussed in this report. At these

in these figures, however, do not give any indication that leading edge vortices exist in these flow fields. This probably means that the leading edge of these blades was not swept forward enough to allow the formation of a leading edge vortex at these low power operating conditions.

The absence of leading edge vortices in the wake flow set up by the forward–swept blades is also indicated by figure 11. Contours of axial vorticity computed from the axial station 2A data are shown for each of the two operating conditions. Also depicted on each plot are the secondary velocities from which the axial vorticity levels were calculated. These contours indicate that the tip vortex is the dominant vortical structure in the wake flow. Vortex sheets are shown to be shed from the trailing edges of the blades, but the peak vorticity levels within the sheets are much lower than those found within the the tip vortices. The relatively high tip vortex strength indicates that the tip regions of these forward–swept blades were highly loaded. Considering how well the tip vortices stand out in these contour plots, it is thought that if leading edge vortices were forming on these blades, that they too would show up in these contours. Since they are not shown, it is evident that no separate leading edge vortices exist in the front rotor wake flow at either operating condition.

As discussed in the introduction section, it was expected that, for a given loading condition, the tips of these forward–swept blades would provide a more uniform tip wake flow than aft–swept blades, and that this would result in decreased interaction noise. The more uniform tip wake flow was expected for a forward–swept blade since, if a leading edge vortex were to form, it would not migrate outboard and merge with the tip vortex. This concept was demonstrated in earlier studies using both a forward–swept stationary vane (ref 1) and a forward–swept rotor (ref 2). In contrast to the data obtained during these previous tests, the F39S blades tested here generated strong tip vortices which produced a very nonuniform wake flow downstream of the blade tips. As shown in a previous paper (ref 3), the axial velocity field generated by these forward–swept blades was more nonuniform than that produced by a conventional aft–swept rotor at the same power loading condition. This forward–swept configuration was also found to generate more interaction noise than a propfan which had aft–swept blades in each rotor. Sideline acoustic data indicated that the interaction tone levels of the forward–swept configuration were up to 8 db higher than those of the conventional aft–swept configuration.

As discussed in Ref 3., the higher interaction noise produced by the forward–swept configuration has been linked to a higher than expected twisting of the blade tips which is thought to have occurred as the model and wind tunnel were brought up to operating speed. Figure 12 shows radial distributions of circumferentially–averaged axial and tangential velocities measured at axial station 2A for both the flutter and below flutter operating conditions. Also shown on the figure are velocity profiles measured in the wake of a reference aft–swept front rotor operating at 6500 RPM with the blade angle, $\beta_{3/4}$, set at 38 degrees. The data measured downstream of this aft–swept front rotor were obtained in a plane 0.63 inches downstream of axial station 2A (0.63 in. represents 8.7% of the 7.22 in. rotor–to–rotor spacing). The figure shows that there are significant differences between the wake flows developed by the two different sets of front rotor blades. The data measured downstream of the aft–swept rotor shows both the axial and tangential components increasing gradually with decreasing radius from the tip until each distribution peaks inboard of 50% span. These data indicate that the aft–swept blade loading peaked at an inboard location and the blade tips were relatively lightly loaded. This is the sort of radial loading distribution that one would expect for a properly designed rotor of a counterrotating configuration. In contrast, the velocity distributions measured downstream of the forward–swept blades show high circumferentially–averaged axial and tangential velocities downstream of the blade

one passage.) The standard deviation of the axial velocities falling within each bin at each radial location was then computed and normalized by the freestream velocity of 220 ft/sec. Finally, the resulting values were made to represent a percentage of the freestream velocity by multiplying by 100. Provided no sources other than turbulence contribute to the measured unsteadiness, the above mentioned standard deviations represent the local axial turbulent velocities. Outside the rotor wake in the freestream, the normalized axial turbulent velocity is equivalent to the axial turbulence intensity. For a number of reasons, however, the computed standard deviations are expected to be biased high relative to the actual local turbulent velocities. These reasons include, flow field unsteadiness created by the blade flutter, passage–to–passage variations in the flow, mean velocity gradients along the length of the LDV probe volume, potential field non–uniformities created by the aft rotor blades, and low frequency oscillations of the tunnel flow. Because of these sources it is thought that the the plotted data do not accurately represent the flow turbulence; they do, however, provide some insight as to how the unsteadiness of the flow varies both locally about the blades and as the operating condition changes from below flutter to flutter. As can be seen from the plots for each condition, the unsteadiness is highest within those regions having the steepest velocity gradients – the tip vortices, the blade wakes and the hub boundary layer. A slight increase in the unsteadiness is shown to occur near the hub just to the right of the viscous blade wake. This may be due to the presence of a hub vortex. The shapes of the unsteadiness contours are similar for the two operating conditions, but as would be expected, during flutter the near–blade region of high unsteadiness is larger and the peak levels are greater. The maximum unsteadiness level measured within the blade wake at flutter approached 28% of the freestream velocity, or 64 ft/sec. At this point in the flow the mean axial velocity was measured to be about 280 ft/sec. If the data measured at this location followed a gaussian distribution, 95% of the axial velocity measurements would fall within a range about the mean of roughly +/– 128 ft/sec (+/– 2 standard deviations). This indicates, as do the other plotted contours, a highly unsteady rotor wake flow – especially in the viscous regions. This should be kept in mind when viewing the phase–locked averaged contour and vector plots, which tend to show nice, smooth variations of the mean flow. These unsteadiness contours indicate that rather severe changes in the flow field can occur over time even when locked in a given position in the rotating reference frame of the front rotor. Nonuniformities significantly greater than those suggested above by the mean, time–averaged views of the wake flow were measured.

Constant Radial Plane Surveys

Figure 15 presents phase–locked averaged axial velocities measured within the blade passages of the front rotor during flutter. Shown are the results of surveys made at six different radial locations between r=10.0 and r=13.0 in. The view depicted is from outside the front rotor blade row looking radially inward. In this view the tunnel flow would be moving from right to left. Constant–radius blade airfoil sections are shown superimposed on the contours. The location and orientation of these sections were subjectively chosen based on where the airfoils seemed to "fit" in the data. The rotation of the blades would move these airfoil sections upward in this view, making the upper side of the blade the pressure surface and the lower side the suction surface. The survey for r=13.0 in., at the left of the figure, shows data measured very close to the blade tip. In fact, the outermost airfoil section is angled slightly such that the leading edge was just outboard, and the trailing edge just inboard, of this radius. This outermost survey shows a band of high speed flow with axial velocities approaching 560 ft/sec on the suction side of the blade back to about 80% chord. This is abruptly followed by a region of retarded flow in which the mean axial velocities drop to levels as low as 40 ft/sec. This transition from high to low axial velocity results from the inward movement of the tip vortex. Upstream of the transition point the center of the vortex is outboard of this radius, and the measurements were obtained in the high axial

the blade passages. It might be possible to determine whether or not this could happen by examining the unsteady variation of the flow about the mean. Figure 18 shows unaveraged data obtained at the location in the flow where the contours of figure 17 indicated that the relative Mach number reached the maximum value of 0.81. Unaveraged axial velocities are plotted vs. the front rotor position in figure 18a, while unaveraged tangential velocities are plotted in figure 18b. This data was obtained during flutter just upstream of the leading edge of the blade at r=12.5 in. The contours of figure 17 indicate that the relative Mach number peaked at this radius at a point where the flow accelerated around the leading edge to the suction side of the blade. The velocities resulting from this acceleration are shown in the unaveraged velocity distributions as the positive and negative peaks in the axial and tangential distributions, respectively. It can be seen from figure 18 that unaveraged axial velocities as high as 500 ft/sec and unaveraged tangential velocities as low as −300 ft/sec were measured in this acceleration region. The combination of these two extreme velocities yields a relative Mach number of 0.90. Assuming both of these components could exist simultaneously, in order for the flow to reach the sonic speed the radial velocity component would be required to have a magnitude of 367 ft/sec. It is unlikely that radial velocities of this magnitude exist at this location in the flow field. Examination of other unaveraged data plots indicate that it is unlikely that the flow within the vicinity of the blades ever became supersonic. Hence it does not appear that shock waves could be responsible for causing the blade flutter.

Conclusions

Data have been presented which illustrate the flow about the forward–swept front rotor blades of a counterrotating propfan operating in a Mach 0.2 freestream at two operating conditions – a condition at flutter, and a condition at which the rpm was reduced just enough to get out of flutter. Based on these data the following observations can be made:

1) Tip vortices were the dominant vortical structures in the wake flow. Leading edge vortices did not form on these forward–swept blades at either operating condition. There is some evidence that hub vortices were generated, but they are much weaker than the tip vortices.

2) Circumferential variations in flow angle measured across the tip vortices were found to be of about the same magnitude as the flow angle variations measured across the viscous blade wakes. This indicates that both the tip vortices and viscous wakes generated by these forward–swept blades would contribute significantly to the generation of interaction noise.

3) The time–averaged flow in the frame of reference of the front–rotor did not undergo any drastic changes as the rotor rotational speed was increased from the below flutter to the flutter operating condition.

4) The flow did not massively separate from the blades during flutter. Therefore, massive blade stall did not cause the flutter.

5) The flow about the blades was subsonic at both operating conditions. Consequently, shock waves did not cause the flutter.

6) The tips of the forward–swept front rotor blades were highly loaded at both operating conditions. This is thought to have been caused by the blade tips twisting under load to higher

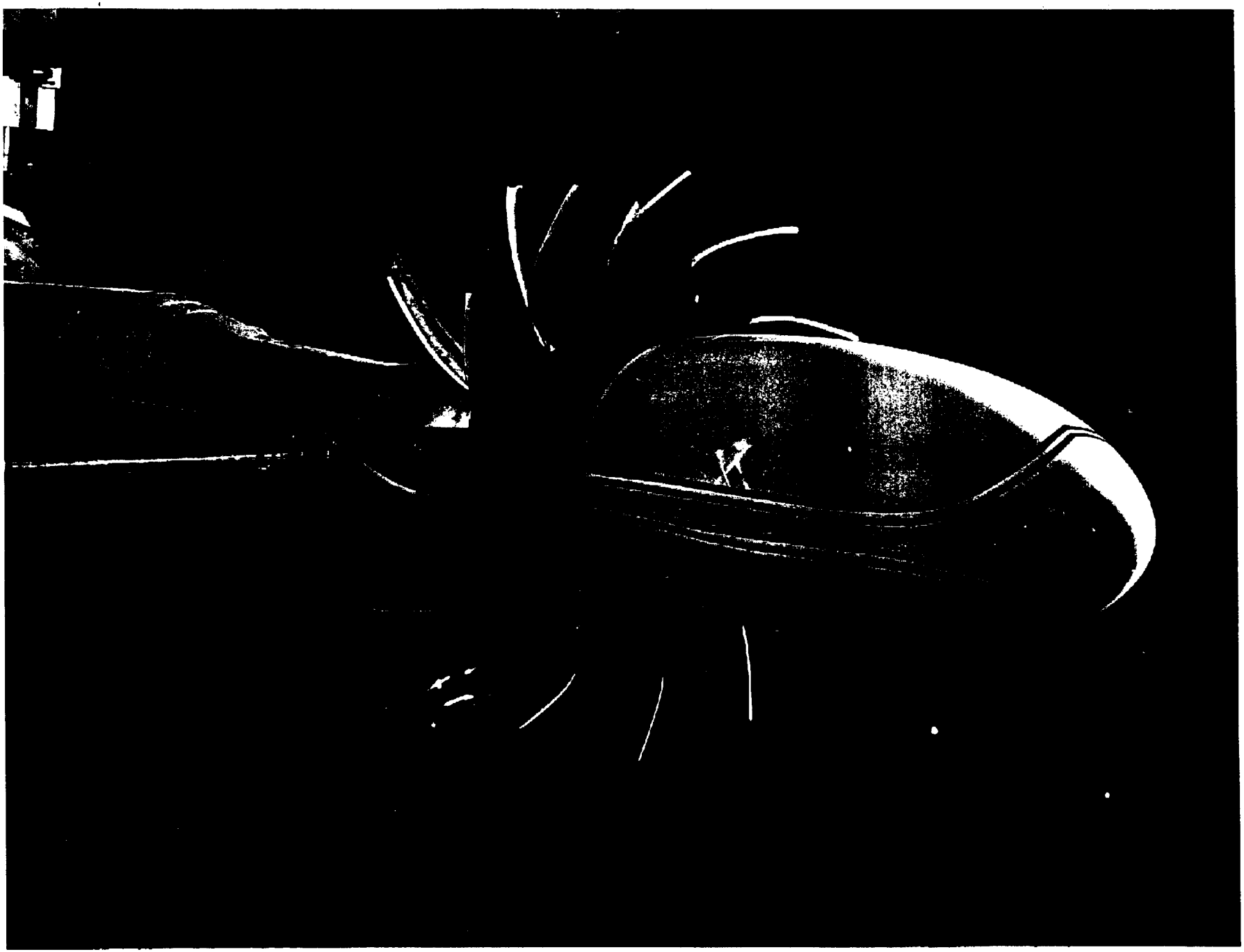

Figure 1.- F39S/A31 propeller blades on model counterrotation propeller test rig installed in the 9 X 15 Foot Wind Tunnel test section.

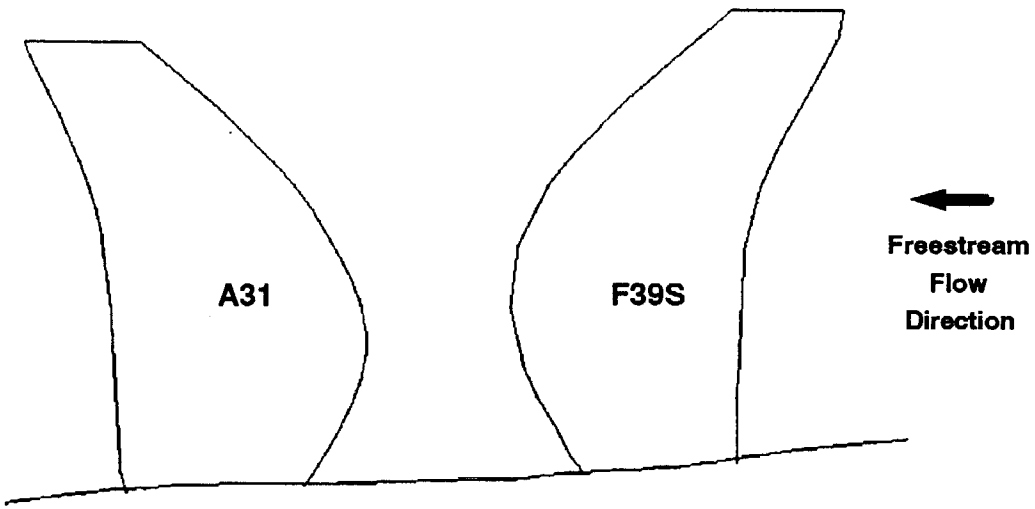

Figure 2.- Planform shapes of front rotor F39S and aft rotor A31 blades.

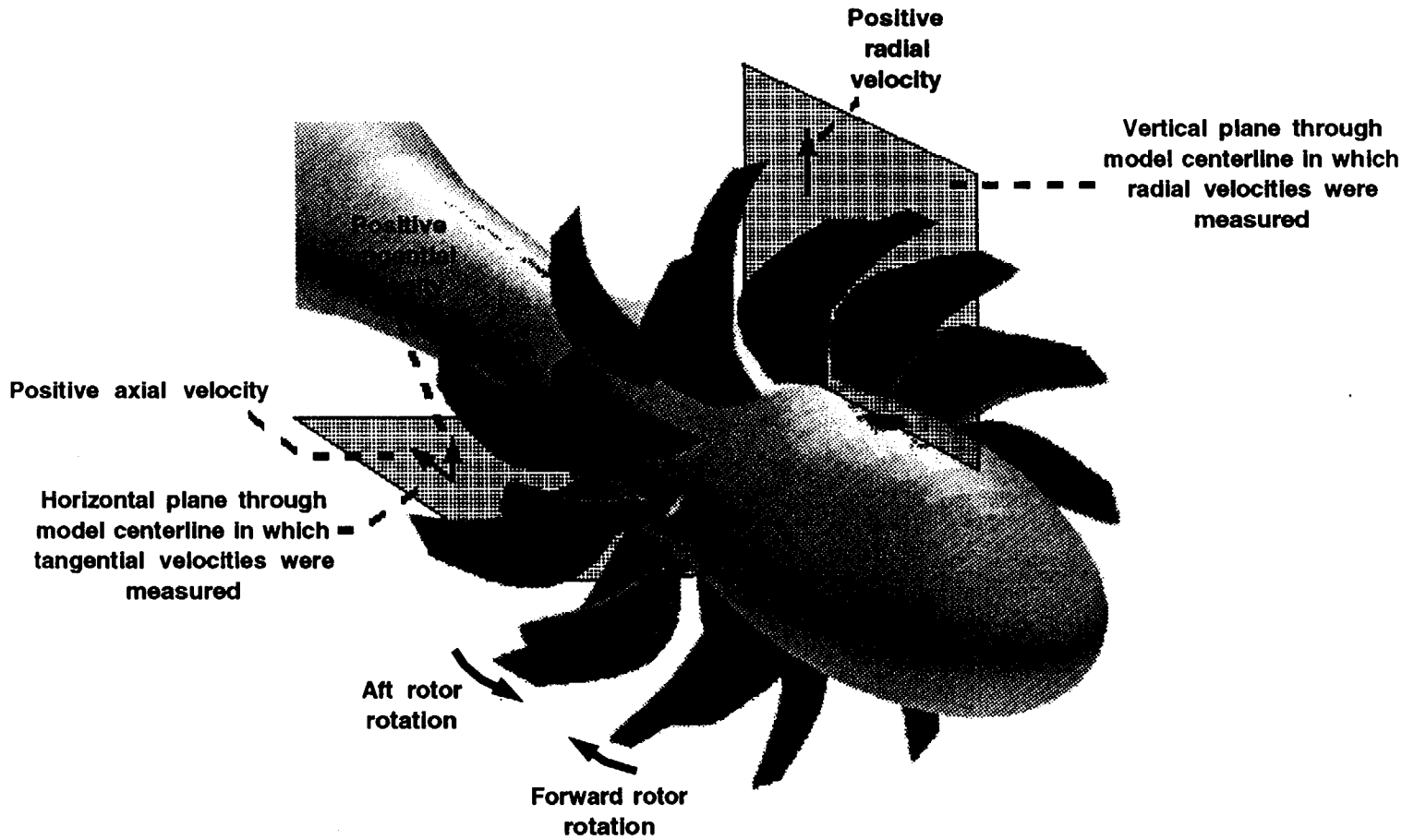

Figure 3.– Schematic of propeller model illustrating horizontal and vertical measurement planes.

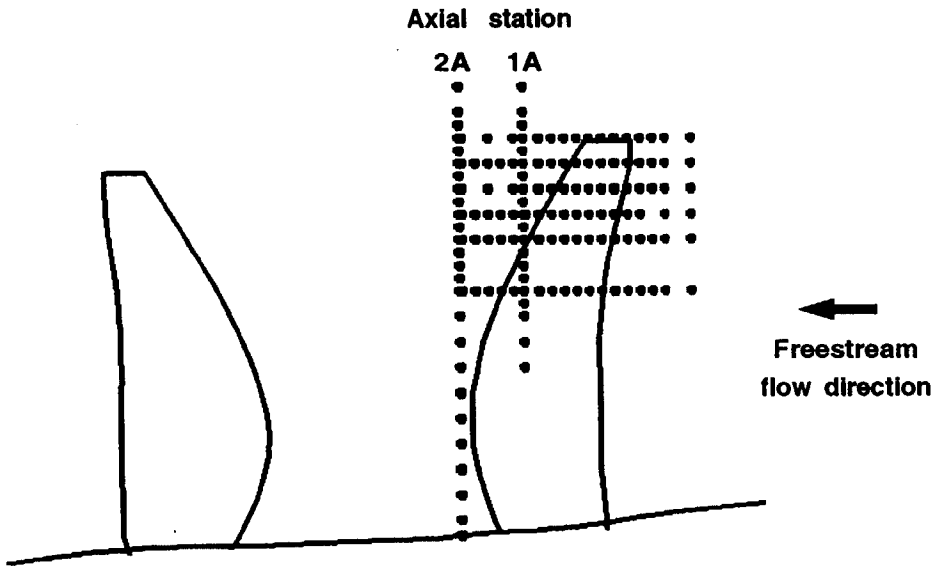

(a) Flutter condition.

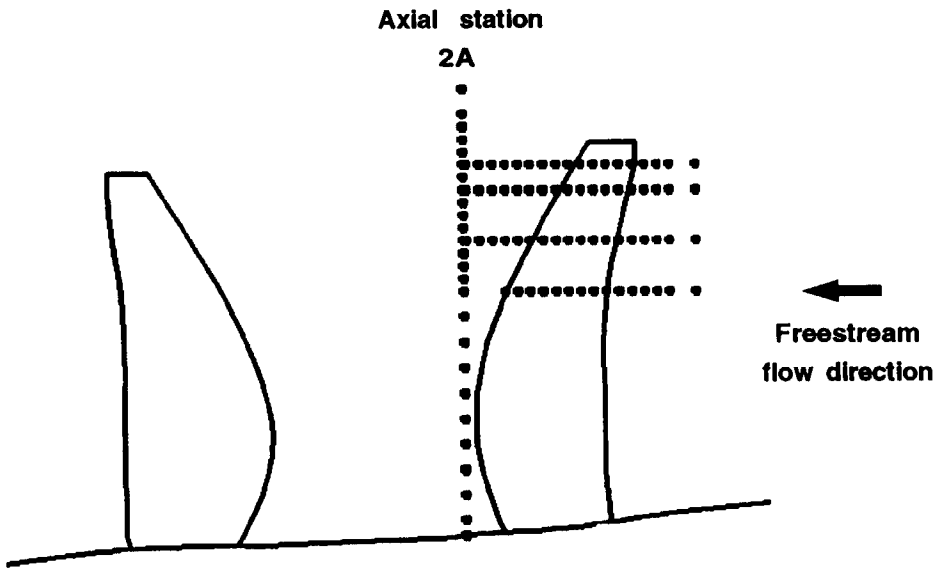

(b) Below flutter condition.

Figure 4.– Schematic showing side view of propeller blades and LDV measurement locations.

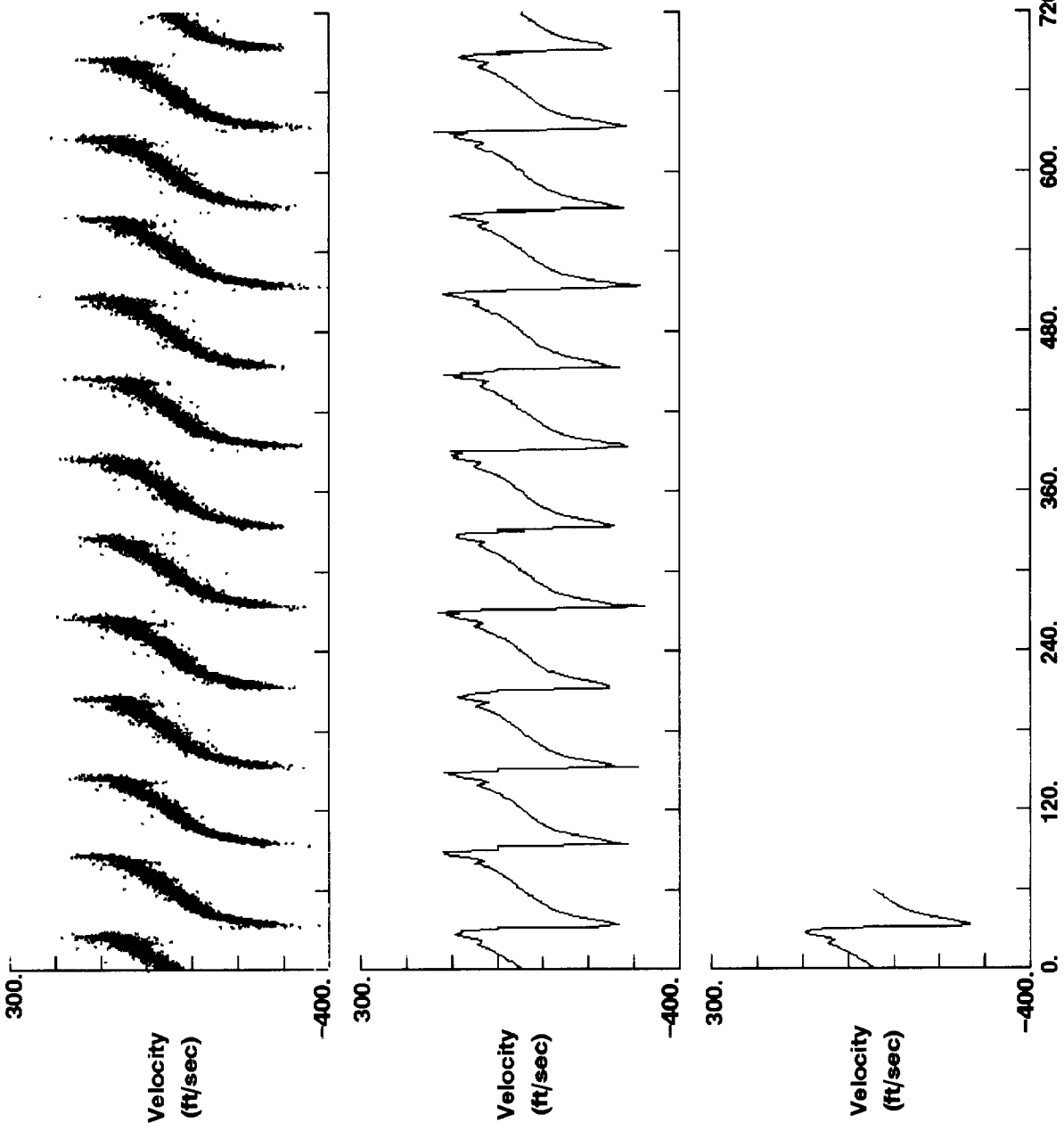

(a) Unaveraged velocities.
(b) Ensemble averaged velocities.
(c) Phase-locked averaged velocities.

Figure 5.- Illustration of LDV data reduction process.

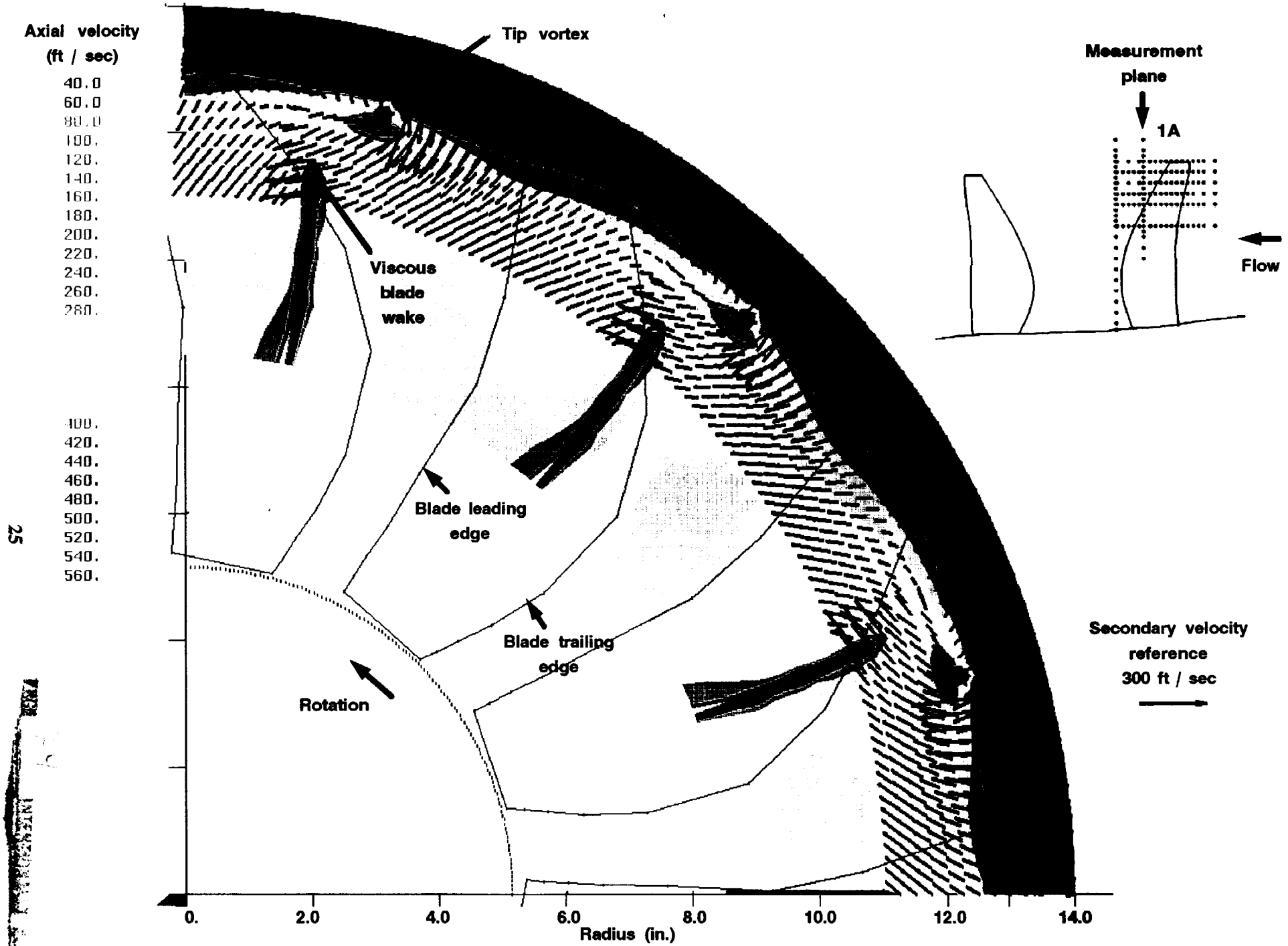

Figure 6.- Phase-locked averaged velocities measured at axial station 1A during flutter (5900 RPM). View is aft of measurement plane looking upstream.

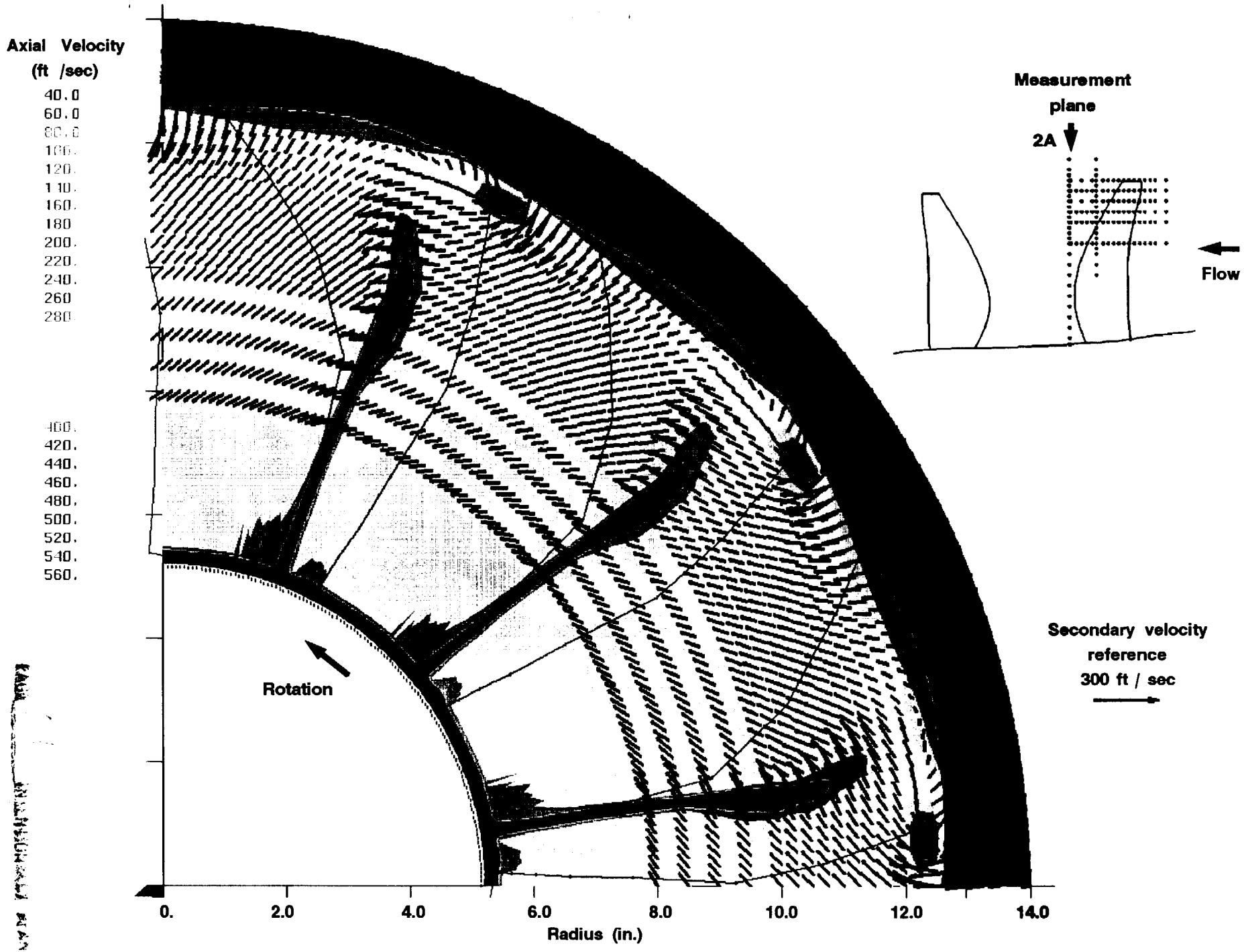

Figure 7.- Phase-locked averaged velocities measured at axial station 2A during flutter (5900 RPM). View is aft of measurement plane looking upstream.

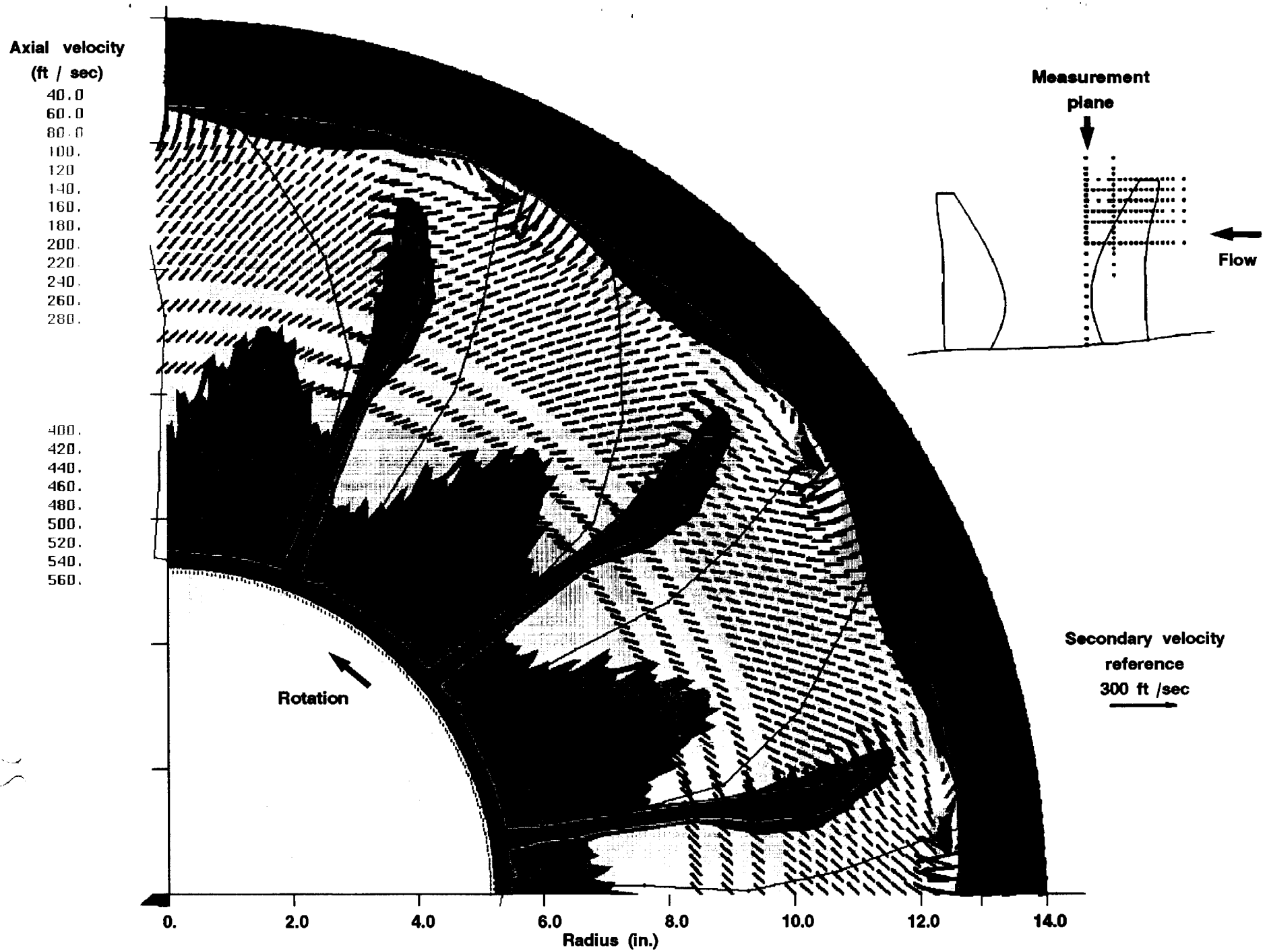

Figure 8.- Phase-locked averaged velocities measured at axial station 2A at the below flutter operating condition (5600 RPM). View is aft of measurement plane looking upstream.

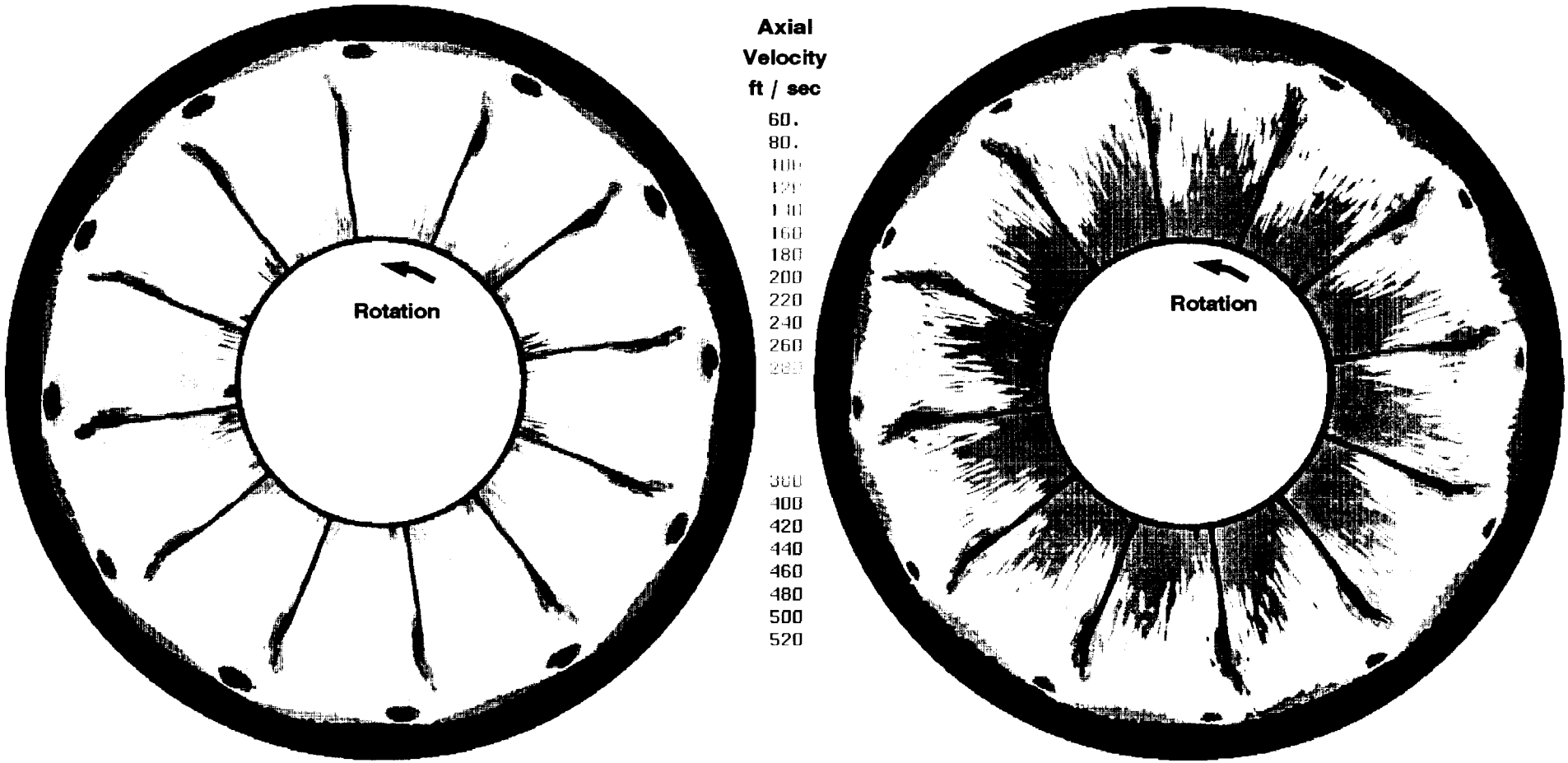

Figure 9.- Ensemble averaged axial velocities measured at axial station 2A for both the flutter and below flutter operating conditions. View is aft of measurement plane looking forward.

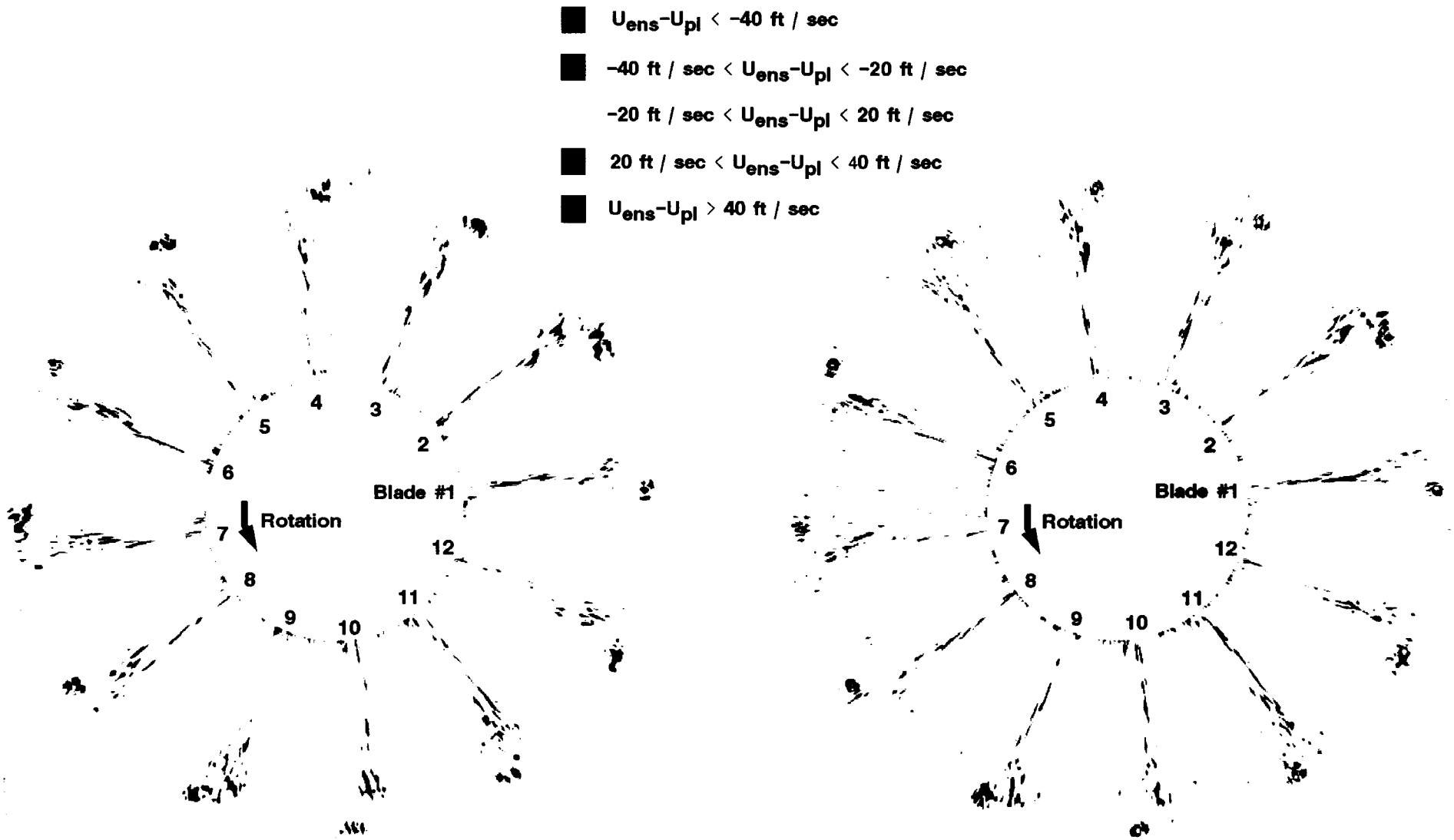

Figure 10.- Variation of the ensemble-averaged axial velocity fields of the individual blade passages from the phase-locked average passage. View is aft of measurement plane looking upstream.

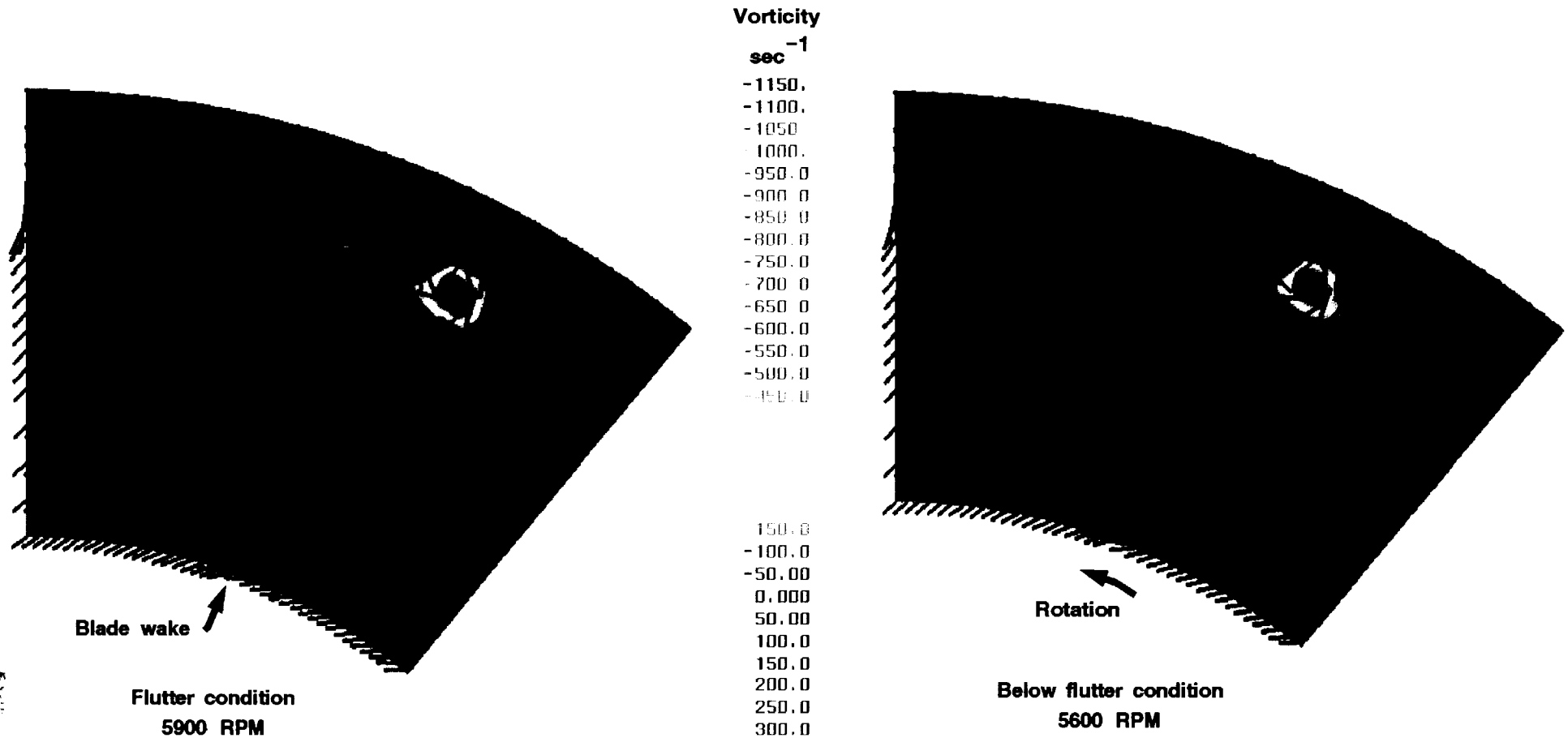

Figure 11.- Axial vorticity contours computed from measured wake flow at station 2A for both flutter and below flutter operating conditions. View is aft of measurement plane looking upstream.

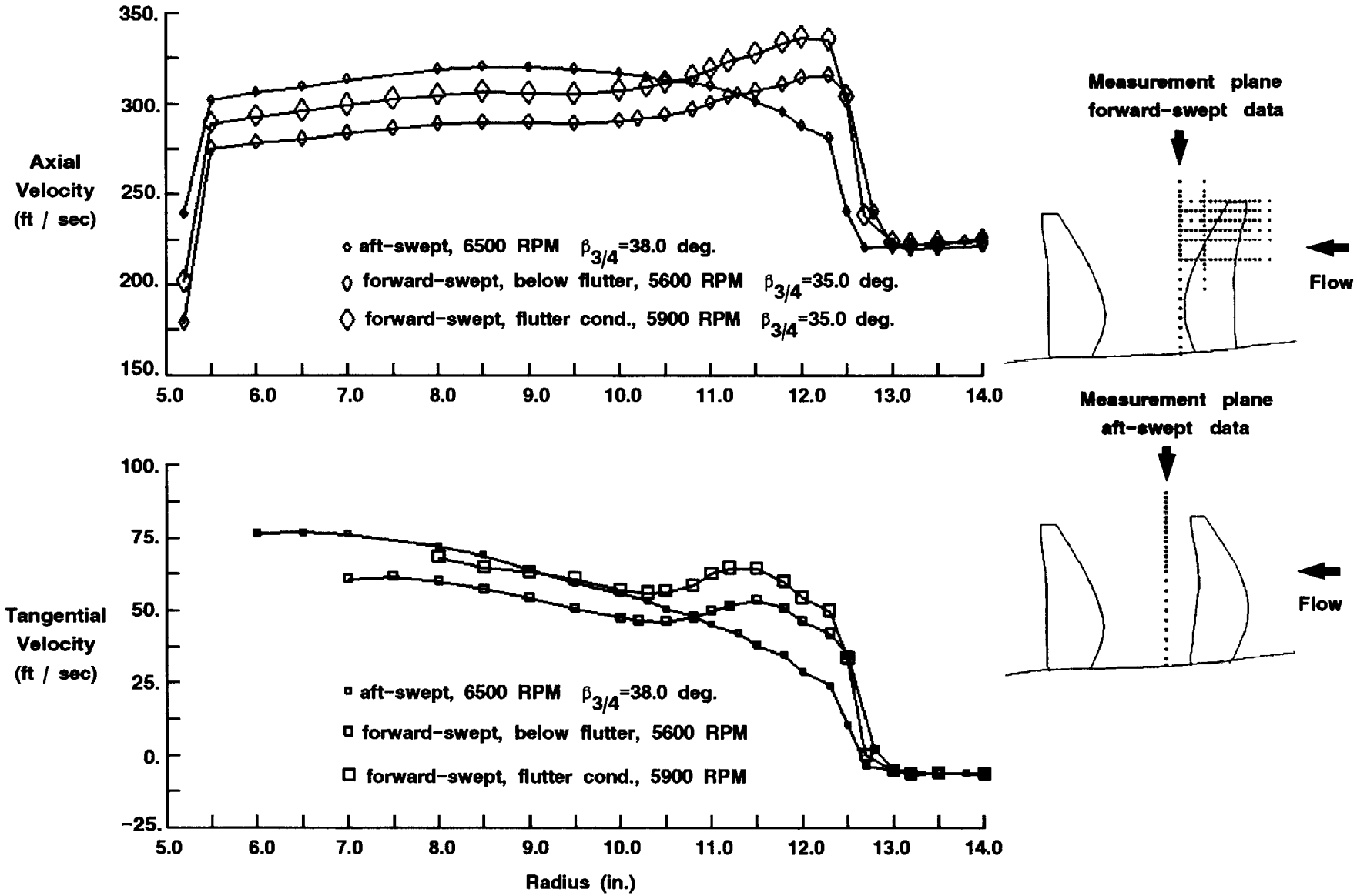

(a) Axial velocity
(b) Tangential velocity

Figure 12.- Comparison of spanwise distributions of circumferentially-averaged velocities measured downstream of forward-swept and aft-swept front rotors.

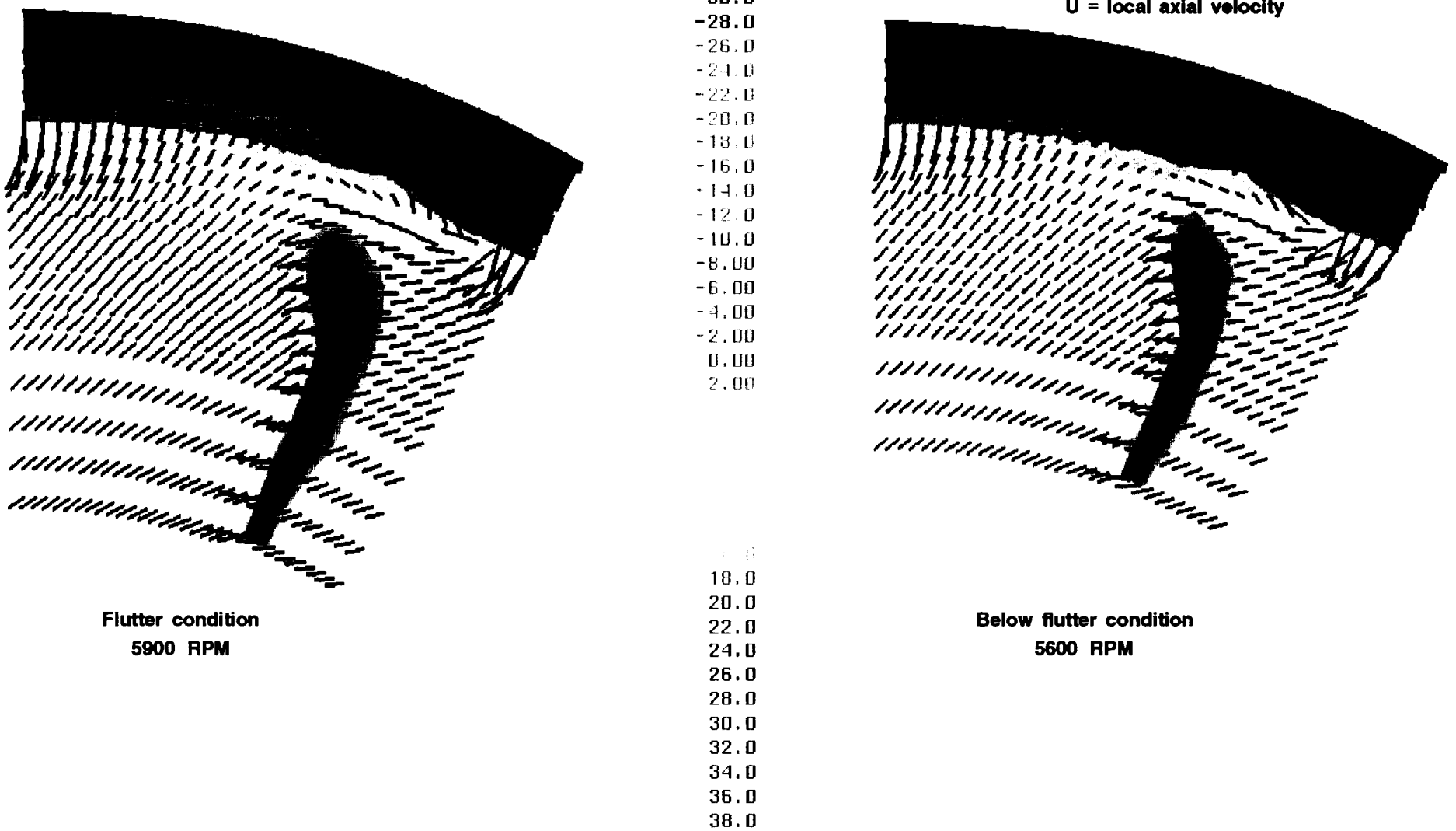

Figure 13.- Flow angle contours computed from measured wake flow at station 2A for both flutter and below flutter operating conditions. View is aft of measurement plane looking upstream.

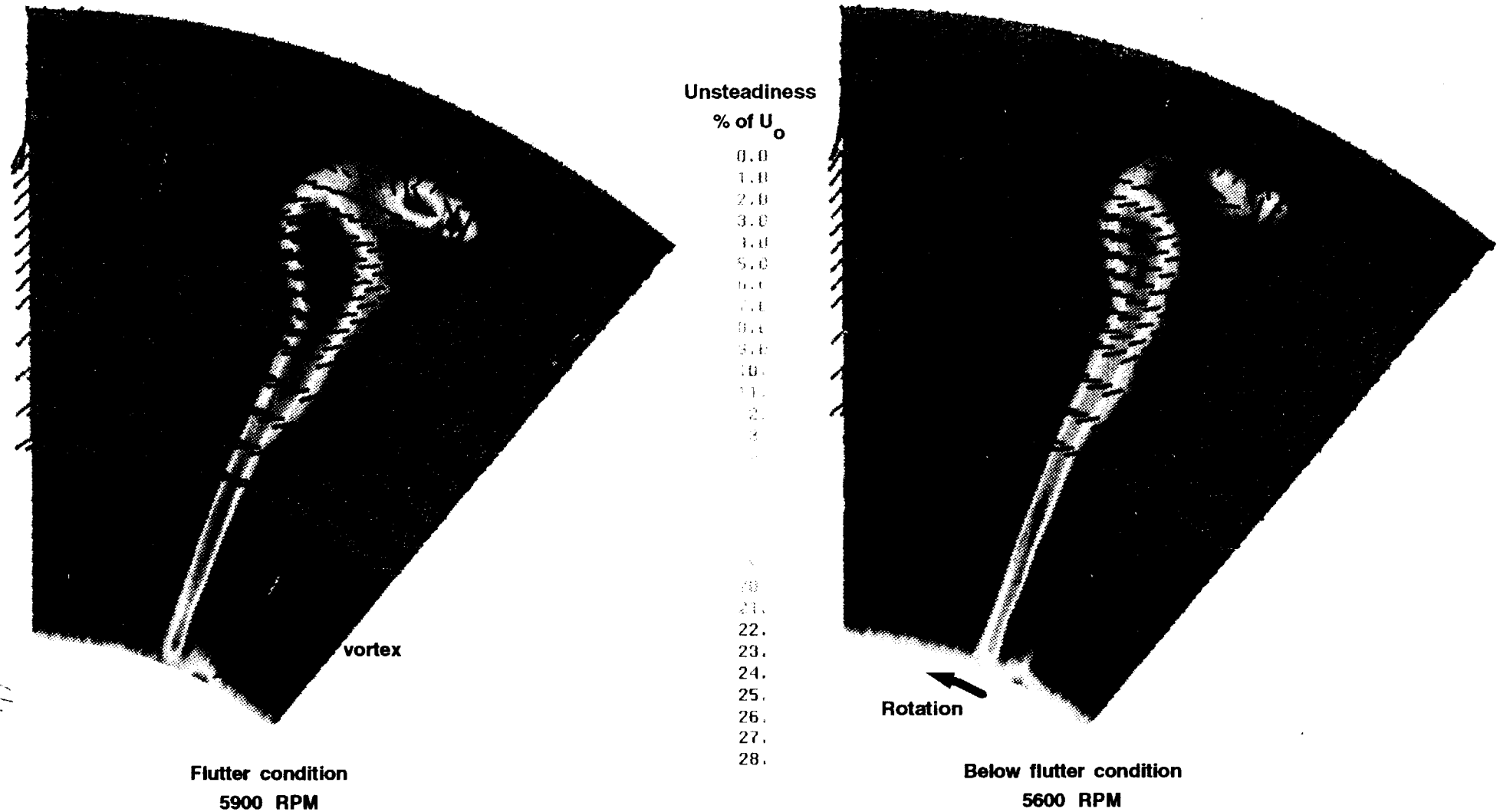

Figure 14.– Axial flow unsteadiness contours computed from measured wake flow at axial station 2A for both the flutter and below flutter operating conditions. Secondary velocity vectors are superimposed on contours. View is aft of measurement plane looking upstream.

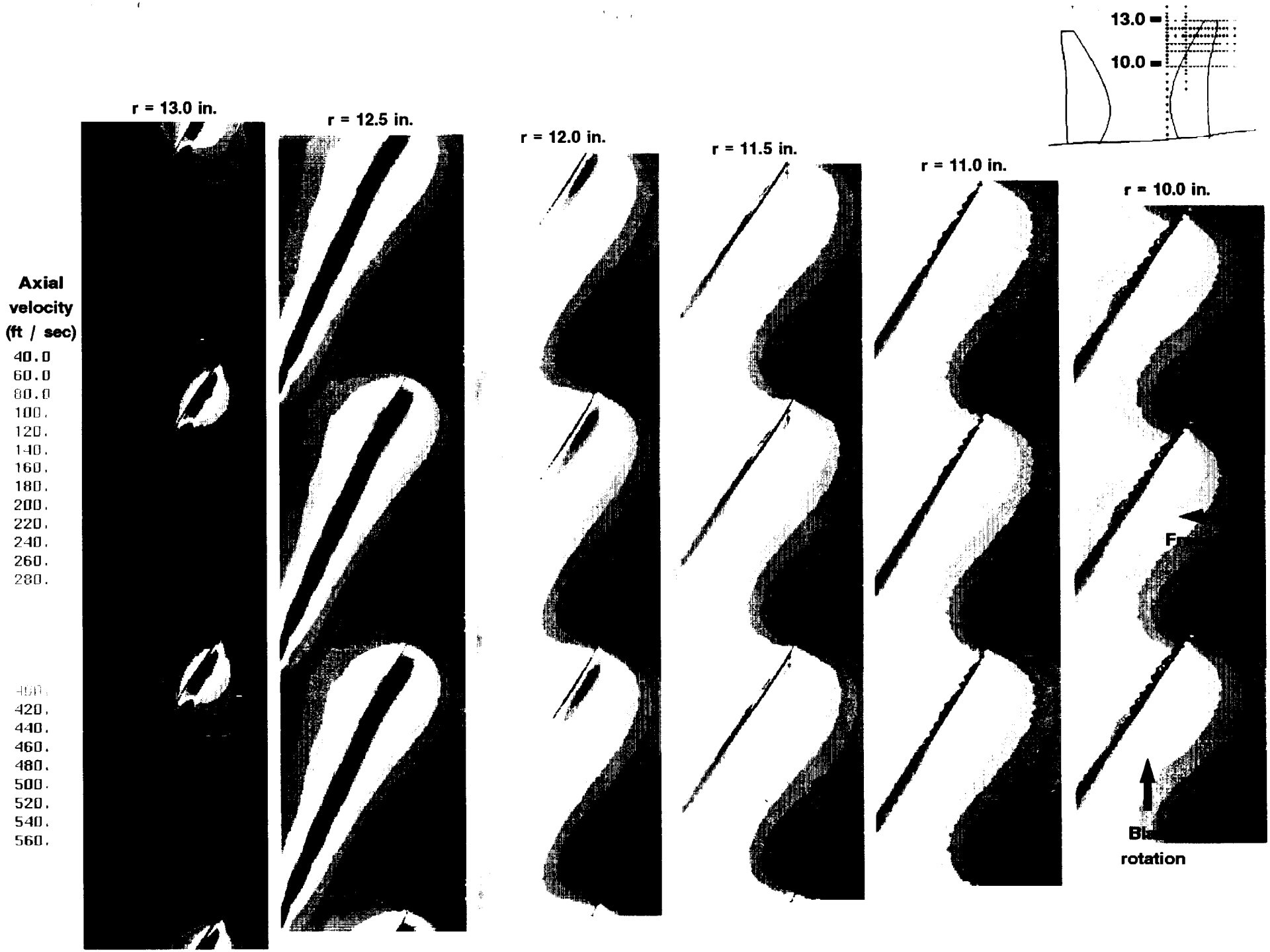

Figure 15.- Intra-blade phase-locked averaged axial velocity contours measured during flutter (5900 RPM).

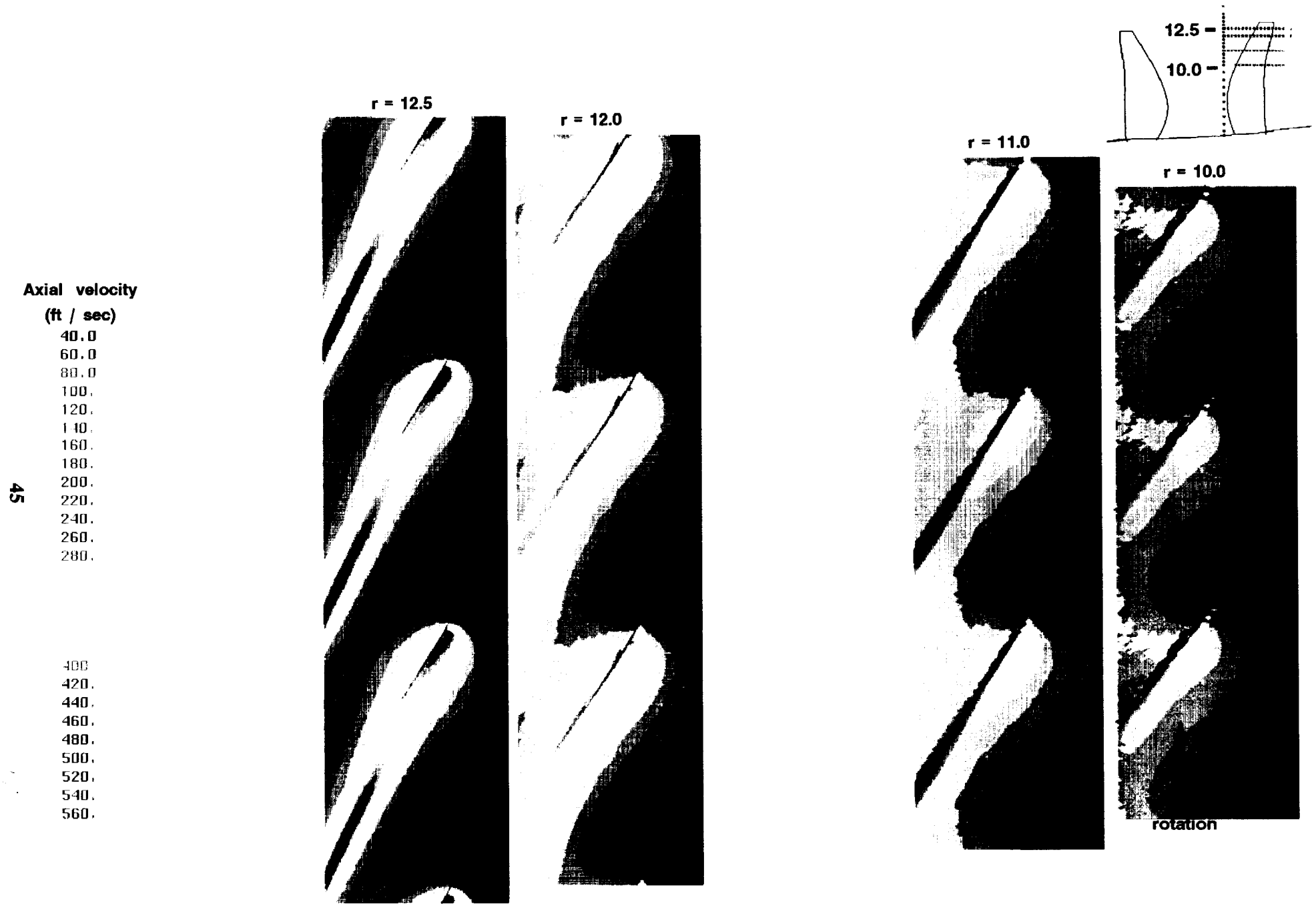

Figure 16.- Intra-blade phase-locked averaged axial velocity contours measured at below flutter condition (5600 RPM).

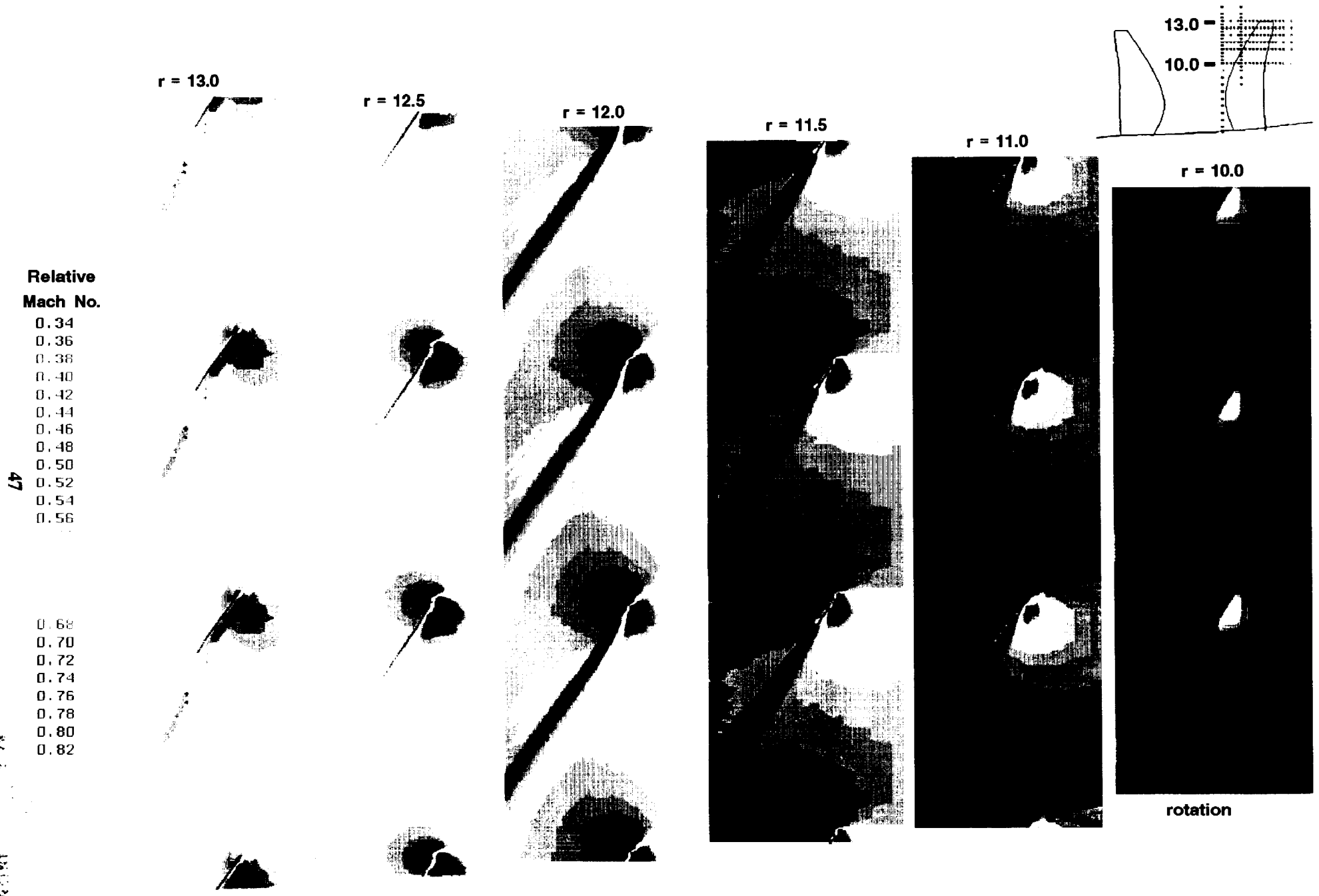

Figure 17.- Intra-blade relative Mach number contours computed from phase-locked averaged axial and tangential velocities measured during flutter (5900 RPM).

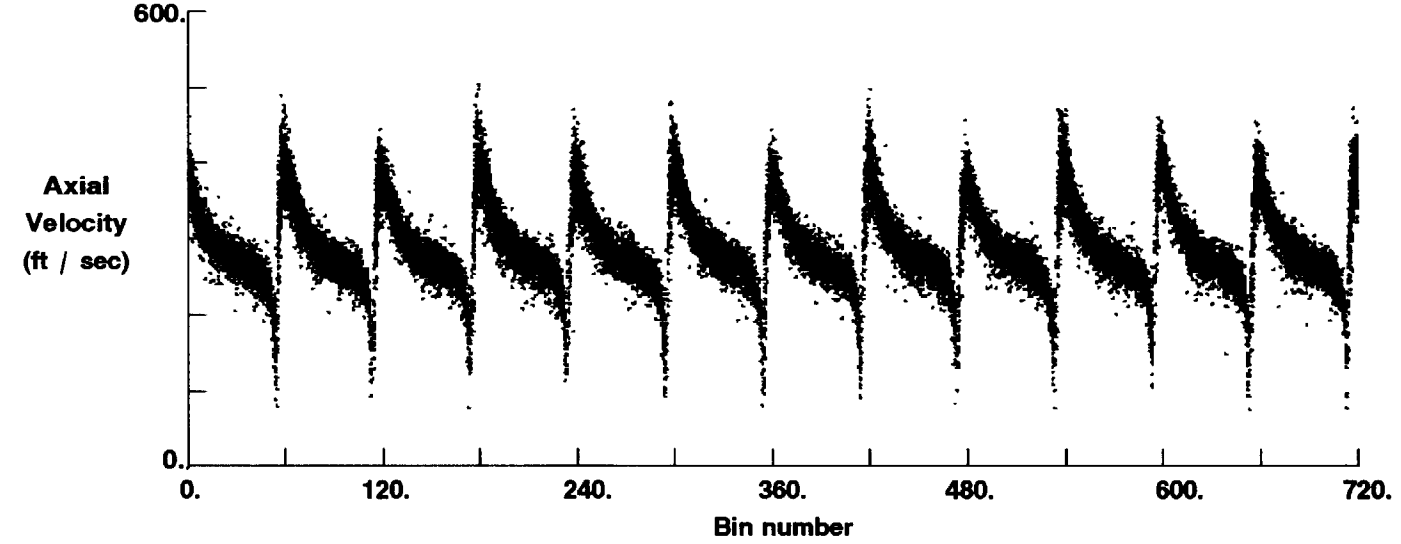

(a) Axial velocity distribution

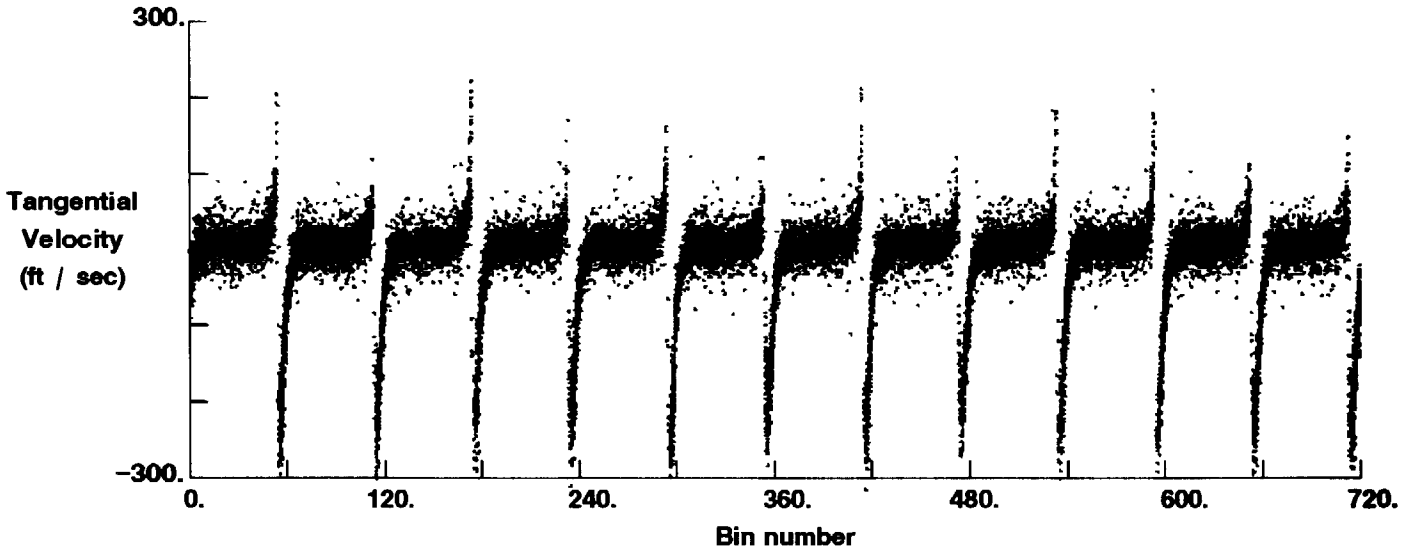

(b) Tangential velocity distribution

Figure 18.- Circumferential distributions of unaveraged axial and tangential velocity measured at r=12.5 in., just upstream of blade leading edge during flutter (5900 RPM).